

TOWARDS A BAPTA MECHANISM FOR SMALL SATELLITES

Mário César Ricci

Sebastião Eduardo Corsatto Varotto

National Institute for Space Research – INPE

Space Mechanics and Control Division - DMC

Av. dos Astronautas, 1758 – Jardim da Granja

12227-010 – São José dos Campos – SP - BRASIL

E-mail: mcr@dem.inpe.br , varotto@dem.inpe.br

Abstract

This work intends to show some aspects about the mechanical layout and modeling of a BAPTA (Bearing and Power Transfer Assembly) mechanism in development involving a government institution (INPE) and private companies. The design here described is being evolved for application in small satellites (~0.5 kW with a rigid solar panel of ~1.0 kgm²). The selected concept uses a conventional 1.8° stepper motor and a 100:1 harmonic drive reduction gearing to achieve a theoretical output step size of 0.018°. Simulations in computer are showing that significant interaction with the solar array and spacecraft can be avoided (spacecraft pitch disturbing velocity is lower than 10⁻³ deg/sec) with power consumption as low as 3 to 5 W. The adequate determination of the power consumption is possible due to a adequate representation of magnetic non-linearity in the motor, including its effect on electromagnetic torque production. The reliable prediction of the important dynamic characteristics of the motor and general system necessitates a precise representation of the flux-linkage data. A good example is the single-step damping, which can be predicted satisfactorily only if the current disturbance and associated power loss in each stator circuit are calculated correctly. This requires that the rate of change of flux-linkage be defined accurately for any combination of the system variables.

Key words: BAPTA, Small satellites, modeling.

Introduction

Some kinds of artificial satellites must be appointed toward the Earth while the solar panels must be appointed toward the Sun in order of maximize the solar energy that reaches the solar panels. These kinds of satellites shall incorporate a BAPTA (Bearing and Power Transfer Assembly) mechanism.

The BAPTA is a Power Subsystem mechanism that performs the tasks of maintain the one degree-of-freedom of the output axis (panel axis) while transmits the electrical and power signals from the panel to the

satellite body. The BAPTA consists basically of three main units: a) the Bearing Unit, b) the Drive Unit and c) the Slip Rings Unit.

The design here described is being evolved for application in small satellites with a rigid solar panel of about 0.5 kW and 1.0 kgm² of inertia. The platform inertia shall be not less than 20 kgm².

In this work we concentrate the efforts in the modeling of the Drive Unit. Two solutions were considered for the Drive Unit: a) closed-loop synchronous system and b) open-loop incremental motion control system. Since the orbital period is too large (on the order of 10² min) the nominal speed and its variation are very low and very difficult to measuring. Therefore, the second solution is to be the better choice and the selected concept uses a conventional 1.8° stepper motor and a 100:1 harmonic drive reduction gearing to achieve a theoretical output step size of 0.018° (Figure 1).

In normal mode the mechanism operates in open-loop with a frequency of about 3.11 steps per second. When the solar panel's normal deviates from Satellite-Sun vector of an angle greater than two degrees a signal is send to the control electronics to modify the system's clock in order to maintain the solar panel's pointing requirements.

The main specifications for the BAPTA mechanism, operating in a satellite with a orbital period of 107 minutes, are given in Table 1.

Table 1: Main Specifications for the BAPTA Mechanism

Orbital mean rate (orbital period of 107 min)	0.056 °/s
Pitch disturbing velocity	< 10 ⁻³ °/s
Solar panel's inertia	1 kg m ²
Platform inertia	20 kg m ²
Total mass	< 2 kg
Power consumption	5 W
Overall dimensions	
Electronic box	120x120x120 mm
Mechanical part	120x120x120 mm

Nomenclature

c	equivalent damping coefficient,
k	spring constant,
k_v	coefficient of viscous friction,
T_f	friction torque,
T	electromagnetic torque,
i	motor current,
J	moment of inertia,
N_r	number of rotor teeth,
R	total series resistance of a stator circuit,
V	voltage applied,
W'	co-energy,

Greeks:

θ	instantaneous angular position,
λ	flux-linkage,
ω	instantaneous angular velocity,

Subscripts:

a	refers to the change in flux-linkage of phase A as a function of i_{AC} and θ ,
A	refers to the motor's phase A,
B	refers to the motor's phase B,
C	refers to the motor's phase C,
D	refers to the motor's phase D,
AC	refers to the current difference between the motor's phases A and C,
BD	refers to the current difference between the motor's phases B and D,
PMA	refers to the change in flux-linkage of phase A due to the permanent magnet as a function of the angular position,
1	refers to the satellite body,*
2	refers to the motor's rotor and reduction gearing input and output axis,
3	refers to the solar panel and yoke,
21	refers to the position and velocity displacements between the rotor and the platform,
32	refers to the position and velocity displacements between the solar panel plus yoke and the reduction gearing output axis.

* nonnegative integers are used as subscript index in coefficients of trigonometric series also

Equations of Motion

The system under investigation consists of a rigid asymmetric platform (with inertia J_1 and attitude θ_1) linked to an axisymmetric body (with inertia J_2 and attitude θ_2), stands for the motor's rotor and reduction gearing, that is connected by a lossy torsional spring to a third axisymmetric body (with inertia J_3 and attitude θ_3), representing the rigid solar panel and the yoke as illustrated in Figure 2.

Disregarding the translational motion of the spacecraft the degrees-of-freedom of the system are θ_1, θ_2 and θ_3 , where the attitude θ_1 is to be controlled with respect to an absolute reference and the masses are free to oscillate about the common axis of symmetry. The equations of motion may be arranged into eight 1st-order differential equations:

$$\frac{d\theta_1}{dt} = \omega_1, \quad (1)$$

$$\frac{d\omega_1}{dt} = -\frac{1}{J_1} \left[T(i_{AC}, \theta_{21}) + T(i_{BD}, \theta_{21}) - k_v \omega_{21} - T_f \frac{\omega_{21}}{|\omega_{21}|} \right], \quad (2)$$

$$\frac{d\theta_2}{dt} = \omega_2, \quad (3)$$

$$\frac{d\omega_2}{dt} = \frac{10^4}{J_2} \left[T(i_{AC}, \theta_{21}) + T(i_{BD}, \theta_{21}) - k_v \omega_{21} - T_f \frac{\omega_{21}}{|\omega_{21}|} \right] + \frac{1}{J_2} (k\theta_{32} + c\omega_{32}), \quad (4)$$

$$\frac{d\omega_3}{dt} = -\frac{1}{J_3} [k\theta_{32} + c\omega_{32}], \quad (5)$$

$$\frac{d\theta_3}{dt} = \omega_3, \quad (6)$$

$$\frac{di_{AC}}{dt} = \frac{1}{\frac{\partial \lambda_A}{\partial i_{AC}}} \left[\frac{V_A - V_C}{2} \right]$$

$$\left. -\frac{Ri_{AC}}{2} - \omega_{21} \frac{\partial \lambda_A}{\partial \theta_{21}} \right], \quad (7)$$

$$\frac{di_{BD}}{dt} = \frac{1}{\frac{\partial \lambda_B}{\partial i_{BD}}} \left[\frac{V_B - V_D}{2} - \frac{Ri_{BD}}{2} - \omega_{21} \frac{\partial \lambda_B}{\partial \theta_{21}} \right], \quad (8)$$

where (1) and (2) are the equations for satellite body; (3) and (4) are representing the rotor axis and reduction gearing; (5) and (6) refers to the solar panel plus yoke and (7) and (8) are the electromagnetic equations for motor currents as described as follow.

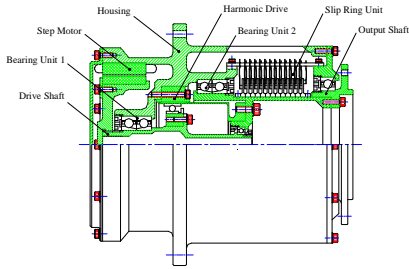


Figure 1: BAPTA mechanism for small satellites

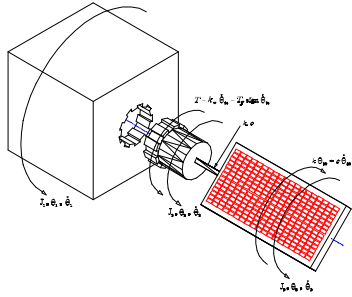


Figure 2: A simplified model for a small satellite with a rigid solar panel

Motor's Model

General Considerations

The motor under consideration here is a low-speed, two phase synchronous inductor motor as described by Snowdon and Madsen^{1,2}. The stator has eight salient poles which are wound with a 2-phase, 4-pole winding. Each salient pole possesses five teeth

having a pitch of one forty-eighth of a revolution. The rotor is constructed of two stacks, each having 50 equally spaced teeth, separated by a axially-magnetized permanent magnet and the teeth on the rotor stacks offset by half a rotor tooth pitch.

To reduce the complexity of the drive circuits the motors are often provided with bifilar windings. The motor may be regarded then as having four independent phases and, instead of reversing the current in a winding, current of the original polarity is supplied to a bifilar coil connected in the opposite sense. This is the arrangement employed in the motor which is the subject of the present work.

With bifilar windings the motor can be thought as a four phase machine and these will be referred to as A, B, C and D respectively. Phases A and C are the two components of one bifilar winding and phases B and D are the two components of the other bifilar winding. With this arrangement, 100% coupling exists between two phases comprising a bifilar pair and currents of the same polarity flowing in the phases A and C, for instance, produce opposing magnetization of the core. Because the quadrature between the two bifilar windings the mutual coupling between them can be considered negligible.

The basic electrical circuit equation, taking phase A as the example, is

$$V_A = Ri_A + \frac{d\lambda_A}{dt}. \quad (9)$$

Considering the coupling between phases A and C (and between the phases B and D) the four differential equations for the electrical circuits are not independent. There are, in fact, just two independent differential equations, one for each bifilar pair of windings. For the bifilar-pair A-C the equation is

$$V_A - V_C = Ri_{AC} + 2 \frac{d\lambda_A}{dt}. \quad (10)$$

The flux-linkage λ_A may be expressed as $\lambda_A(i_{AC}, \theta)$. A similar $\lambda_B(i_{BD}, \theta)$ exists, of course, appropriate to the bifilar-pair B-D. Substituting for λ_A and λ_B , and combining the mechanical equations with those of the electrical circuits, yields the eight 1st-order differential equations (1-8).

The expression for the flux-linkage of each pair of bifilar coils, in terms of net coil current i and the angular position of the rotor θ , may be determined according to Pickup and Russel³, by fitting

mathematical functions to experimental flux-linkage data obtained from static tests. As indicated previously, in order to use the model for prediction of the dynamic response, it is necessary to be able to specify $\partial\lambda/\partial i$, $\partial\lambda/\partial\theta$ e $T(i,\theta)$, given instantaneous values of the variables i and θ .

Taking phase A, for example, the flux-linkage can be expressed as

$$\lambda_A(i_{AC},\theta) = \lambda_{PMA}(\theta) + \lambda_a(i_{AC},\theta). \quad (11)$$

Here, $\lambda_{PMA}(\theta)$ is a flux-linkage of phase A due to the permanent magnet flux when the net current in bifilar pair A-C is zero. $\lambda_a(i_{AC},\theta)$ represents the change in flux linkage of phase A which occurs owing to the flow of a net current i_{AC} in the coils of that phase.

Provided that $\lambda_{PMA}(\theta)$ and $\lambda_a(i_{AC},\theta)$ are continuous functions, $\partial\lambda_a/\partial\theta$ and $\partial\lambda_a/\partial i_{AC}$ can be obtained directly by differentiation of equation (11). The electromagnetic torque $T(i_{AC},\theta)$ can be calculated from the magnetic co-energy $W'(i_{AC},\theta)$. The co-energy is given by

$$W'(i_{AC},\theta) = \int_0^{i_{AC}} \lambda_a(i'_{AC},\theta) di'_{AC}, \quad (12)$$

where i'_{AC} is a dummy variable.

Substituting equation (11) into equation (12) yields

$$W'(i_{AC},\theta) = \lambda_{PMA}(\theta) i_{AC} + \int_0^{i_{AC}} \lambda_a(i'_{AC},\theta) di'_{AC}. \quad (13)$$

The torque produced is then given by

$$T(i_{AC},\theta) = \left. \frac{\partial W'}{\partial \theta} \right|_{i_{AC}=cte}. \quad (14)$$

Substituting equation (13) for the co-energy, into equation (14), and performing the differentiation, gives

$$T(i_{AC},\theta) = i_{AC} \frac{d\lambda_{PMA}(\theta)}{d\theta}$$

$$+ \frac{\partial}{\partial \theta} \int_0^{i_{AC}} \lambda_a(i'_{AC},\theta) di'_{AC}. \quad (15)$$

Thus, the torque consists of two components. The first term of equation (15), can be thought of loosely as the torque produced by the interaction of the permanent magnet flux and the coil current i_{AC} . Similarly, the second term, may be considered to result from the interaction of the current-dependent flux-linkage and the coil current.

The derivatives of the flux-linkage of phase B, $\partial\lambda_B/\partial\theta$ and $\partial\lambda_B/\partial i_{BD}$, and the torque $T(i_{BD},\theta)$ from bifilar pair B-D, can be calculated, of course, in precisely the same manner.

Mathematical Representation of Flux-linkage

Permanent Magnet Flux-linkage

The flux-linkage of phase A from the permanent magnet is symmetrical about the stable zero-torque position ($N_r\theta=0^\circ$) and the unstable zero-torque position ($N_r\theta=180^\circ$), and is equal and opposit about $N_r\theta=90^\circ$, with N_r being the number of rotor teeth. Thus, the following function (with n an odd integer) is suitable for $\lambda_{PMA}(\theta)$:

$$\lambda_{PMA}(\theta) = \lambda_1 \cos(N_r\theta) + \lambda_3 \cos 3(N_r\theta) + \dots + \lambda_n \cos n(N_r\theta). \quad (16)$$

To obtain the experimental flux-linkage readings, taken with zero stator excitation, a stable zero torque position for phase A was located and this was employed subsequently as the reference position. With the machine unexcited and the rotor clamped, the stator was rotated through a given angle and the associated change of flux-linkage recorded on a fluxmeter connected across the windings of phase A (or C). Having recorded the value of flux-linkage, the stator was returned to its reference position and the fluxmeter reset to zero. The test was repeated then for a different value of angular displacement. A similar flux-linkage characteristic can be obtained for phase B, with the reference position displaced by 1.8° ($N_r\theta=90^\circ$).

To fit equation (16) directly to the permanent magnet data, a coefficient λ_0 must be included in the expression to allow for the fact that the reference (zero) level of flux-linkage has been taken at value of

$N_r\theta=0^\circ$ where the absolute flux-linkage of phase A is at a maximum value (obviously this procedure is not necessary if $N_r\theta=90^\circ$, the position where, by symmetry, the absolute value of permanent-magnet flux-linkage of phases A and C is zero, is taken as the reference from which the change of flux-linkage is measured).

The coefficients of equation (16) were determined from the experimental points using the least-square-error method of curve fitting. It was found that the content of harmonics above the third is negligible and, therefore, the following function can be taken to represent adequately the flux-linkage data

$$\lambda_{PMA}(\theta) = \lambda_1 \cos(N_r\theta) + \lambda_3 \cos 3(N_r\theta). \quad (17)$$

This function gives an average discrepancy per experimental point of 0.14×10^{-3} Vs, which is comparable with the experimental accuracy of measurement. The appropriate coefficients of equation are $\lambda_1 = 7.45 \times 10^{-3}$ Vs and $\lambda_3 = 5.14 \times 10^{-5}$ Vs. The Figure 3 shows the experimental measurements and theoretical representation from curve fit for the permanent magnet flux-linkage.

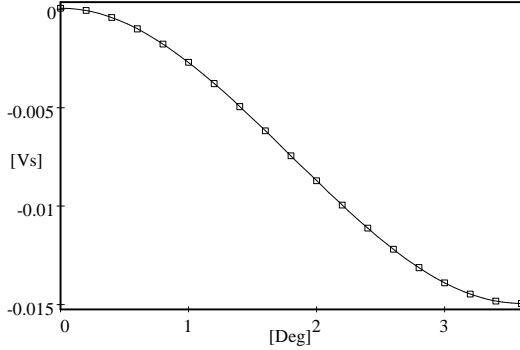


Figure 3: Permanent magnet flux-linkage. Experimental and theoretical values

Current-dependent Flux-linkage

The current-dependent linkage of phase A was measured by using the bifilar-wound coils of phase C as a closely-coupled search coil connected to a fluxmeter. Because of the equal number of turns on phases A and C this arrangement gives a direct reading of the flux-linkage changes which occur in phase A.

Initially the rotor and stator were set up in the reference position ($N_r\theta=0^\circ$) as defined in previous sub-section. A positive current of 0.5 A was switched on in phase A and the associated change in the flux-linkage was recorded on the fluxmeter connected to the bifilar winding. This reading gives the current-dependent flux-linkage at $N_r\theta=0^\circ$ for 0.5 A of positive excitation. The current-dependent flux-linkage at other positions of rotor relative to stator was obtained in a similar manner. The complete test was then repeated for several different values of positive phase current.

The flux-linkage can be modelled by fitting a mathematical function to the experimental current-dependent data. The flux-linkage corresponding to negative values of current can be calculated directly from this function, as will be indicated later.

A general expression for the flux-linkage, bearing in mind that $\lambda_a(i_{AC}, \theta)$ must be an odd function of i_{AC} and be symmetrical in $N_r\theta$ about $N_r\theta=0^\circ$ and $N_r\theta=180^\circ$, is

$$\lambda_a(i_{AC}, \theta) = \sum_{r=0}^k (B_{1r} i_{AC} + B_{3r} i_{AC}^3 + \dots + B_{jr} i_{AC}^j) \cos r(N_r\theta), \quad (18)$$

where j is an odd integer.

The optimum values of the $[(j+1)/2](k+1)$ coefficients for a given combination of j and k can be determined using an adapted version of least-square-error method. It was found that, on the bases of economy of computing and accuracy of representation, it is necessary to have $j=5$ and $k=2$. Further increasing the degree of the i_{AC} polynomials improves the accuracy marginally. Harmonics in $N_r\theta$ above the second are negligibly small. The Table 2 shows the coefficients obtained by the least-square method and the Figure 4 shows the current-dependent flux-linkage fitting as a function of angular position.

The chosen function gives an average discrepancy per experimental point similar to that obtained for the permanent-magnet flux-linkage. The flux-linkage for negative values of i_{AC} in phase A (which is equivalent to positive current in phase C) are obtained by substituting the appropriate i_{AC} into equation (18) and replacing $N_r\theta$ by $N_r\theta - \pi$.

Additional tests were performed to determine whether or not coupling between the bifilar pairs A-C and B-D was significant. Various levels of direct current excitation were applied to phase B and the measurements of current-dependent flux-linkage in phase A were repeated. It was found that at highest level of excitation used (7 A) the readings obtained were virtually unaffected by the presence of the current in phase B. It can be assumed, therefore, that the common return flux paths in the back of stator core were not significantly magnetically non-linear at this level of stator excitation.

Table 2: Current-dependent flux-linkage fitting coefficients

r	$B_{1r} \times 10^{-3}$	$B_{3r} \times 10^{-5}$	$B_{5r} \times 10^{-7}$
0	6.234470	-2.49055	0.858076
1	-0.917669	-1.94243	3.29916
2	-0.170484	0.925831	-1.10692

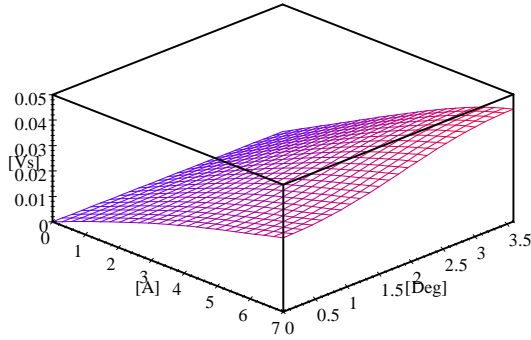


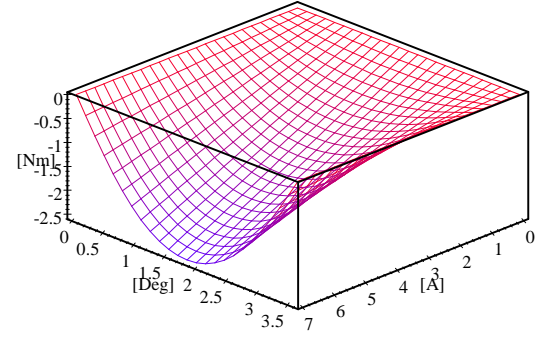
Figure 4: Current-dependent flux-linkage fitting

Static Torque/Angle Characteristics

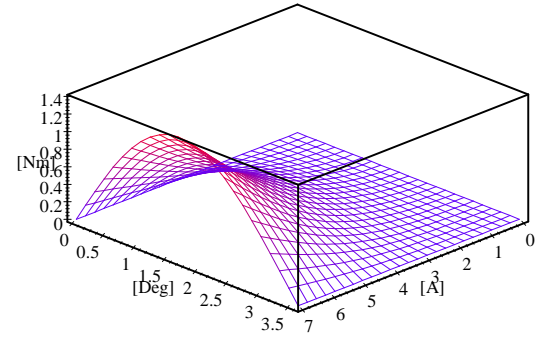
In order to solve the simultaneous dynamics equations (1-8), the electromagnetic torque of the machine is required in terms of instantaneous values of the coil currents and angular position of the rotor. This can be calculated from the flux-linkage. With the functions $\lambda_{PMA}(\theta)$ and $\lambda_a(i_{AC}, \theta)$ derived previously, the torque expression for a single phase becomes

$$T(i_{AC}, \theta) = -N_r \left\{ i_{AC} \left[\lambda_1 \sin(N_r \theta) + 3\lambda_3 \sin 3(N_r \theta) \right] + \sum_{r=1}^2 r \left(B_{1r} \frac{i_{AC}^2}{2} + B_{3r} \frac{i_{AC}^4}{4} + B_{5r} \frac{i_{AC}^6}{6} \right) \sin r(N_r \theta) \right\}. \quad (19)$$

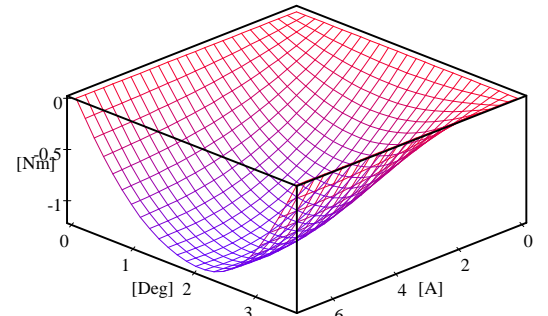
Thus, the two torque components calculated from equation (15) can be evaluated to yield the static torque/angle characteristics at various levels of stator excitation. The Figures 5(a) and 5(b) displays the two torque components using the flux-linkage coefficients. The sum of the components is plotted in Figure 5(c).



(a)



(b)



(c)

Figure 5: Static Torque/Angular Position Characteristics. Due to (a) $i_{AC} d\lambda_{PMA}(\theta)/d\theta$; (b)

$$\frac{\partial}{\partial \theta} \int_0^{i_{AC}} \lambda_a(i_{AC}, \theta) di_{AC}; \text{ (c) the sum of the two}$$

components.
Numerical Results

Some preliminary results are shown in this section. Since it is the qualitative behavior of solutions that is of interest, the results are presented here in graphical form. The computations were performed using a software for simulating dynamic systems named SIMULINK™⁴ that is an extension to MATLAB™⁵. SIMULINK works with windows called *block diagram*. In these windows the model is created and edited by mouse commands. After definition of the model it can be analysed by simulation algorithms and the progress of the simulation can be viewed while the simulation is running. The results can be made available in the MATLAB workspace when the simulation is complete.

The following system's parameters are assumed for the model (1-8) as shown in Table 3.

Table 3: System's parameters

J_1	20.0 Kgm ²
J_2	0.01 Kgm ²
J_3	0.8 Kgm ²
k	125.0 Nm/rd
c	0.1 Nms/rd
T_f	0.05 Nm
k_v	0.0005 Nms/rd
V	30 V
R	200 Ω

The results of simulation are shown in Figures 6-13 and are appropriate to 2-phase excitation using the switching sequence indicated in Table 4.

Table 4: Sequence of excitation for hybrid motor

Step	Phase A	Phase B	Phase C	Phase D
1	On	On	Off	Off
2	On	Off	Off	On
3	Off	Off	On	On
4	Off	On	On	Off

Figures 6 and 7 show the platform angular velocity. It can be seen that the spacecraft pitch disturbing velocity is on order of 10⁻⁵ deg/sec.

Figures 8 and 9 show the net current i_{AC} . The same magnitude inverted profile it was found to i_{BD} .

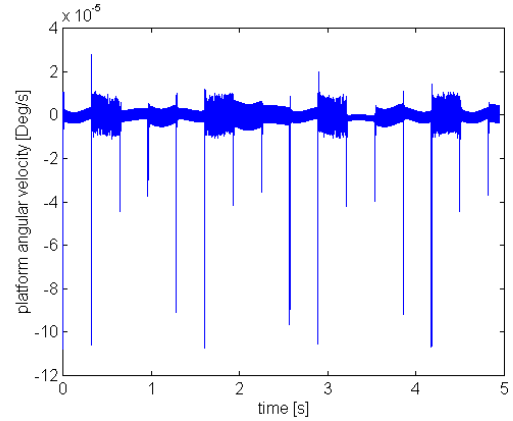
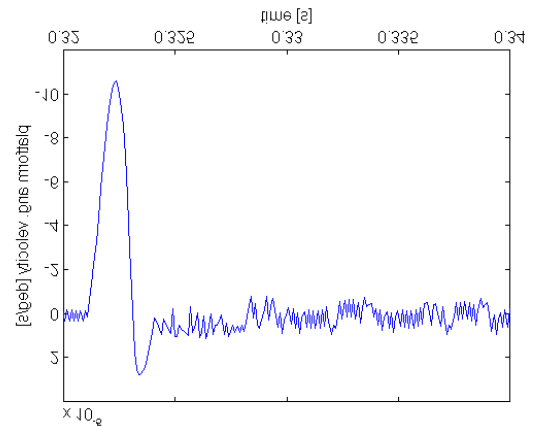


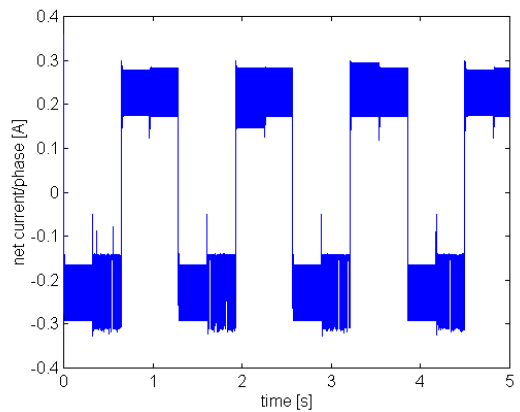
Figure 10 shows the driver's power consumption estimate in watts/phase. It is possible to decrease these

Fig. 6: Spacecraft pitch disturbing velocity



values by a factor of three (and even more) by increasing R or switching off the motor current after the

Fig. 7: Spacecraft pitch disturbing velocity (detail)



settling time has been achieved. The use of the model can be extended to study the effects of using dual-voltage supplies or chopped excitation too.

Fig. 8: Net current i_{AC}

age supplies or chopped excitation too.

Figure 11 shows the motor torque $T(i_{AC}, \theta)$. The same inverted profile it was found to $T(i_{BD}, \theta)$. It can observe an average motor torque of about 0.06 Nm under normal operation.

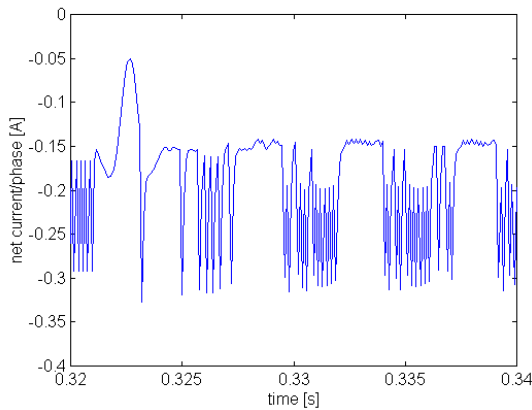


Fig. 9: Net current i_{AC} (detail)

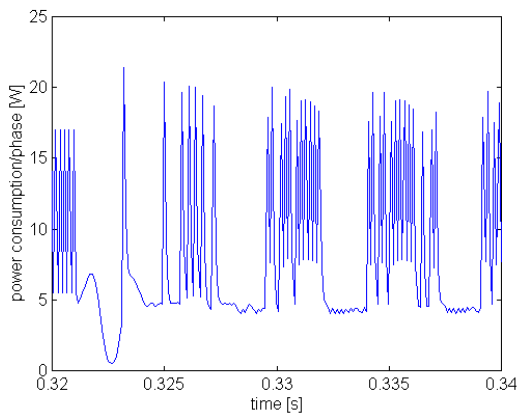


Fig. 10: Power consumption/phase (detail)

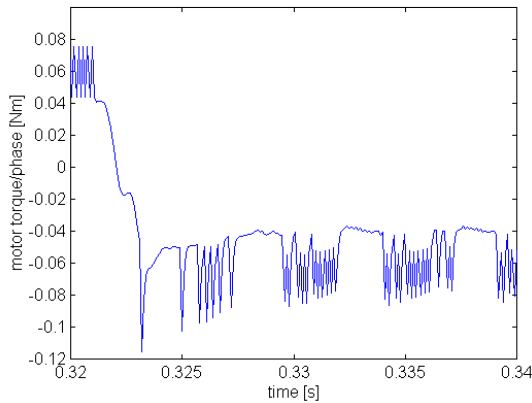
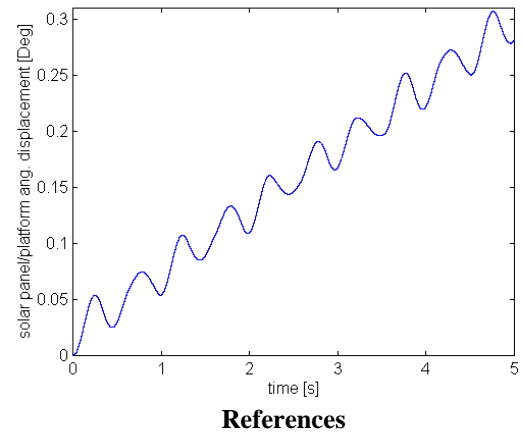
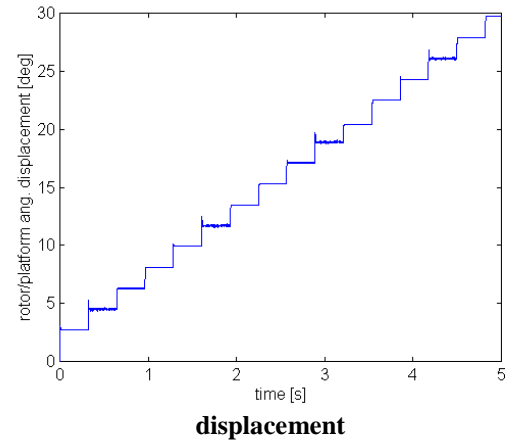


Fig. 11: Motor torque $T(i_{AC}, \theta)$ (detail)

Finally, Figures 12 and 13 show the relative motor's rotor and solar array angular displacements as having the spacecraft as a reference.

Fig. 12: Motor's rotor/platform angular displacement

Fig. 13: Solar panel/platform angular displacement



¹Snowdon, A. E.; Madsen, E. W. Characteristics of a Synchronous Inductor Motor. *Trans. Amer. Inst. Elect. Engrs.*, 1962, IGA-81, pp. 1-5.

²Ricci, M. C. Motor Síncrono de Indução: Características Construtivas e Operacionais. São José dos Campos, INPE, ago. 1986, 42 p. (INPE-3976-RPE/517).

³Pickup, I. E. D.; Russel A. P. A Model for Predicting the Dynamic Characteristics of Hybrid (Permanent Magnet) Synchronous/Stepping Motors. *Proceedings of 9th Annual Symposium on Incremental Motion Control Systems and Devices*, University of Illinois, 1980, pp. 1-13.

⁴SIMULINK A Program for Simulating Dynamic Systems. *User's Guide*, The MathWorks, Inc.

⁵MATLAB *User's Guide*, The MathWorks, Inc.